Check for updates

Electron transport layer assisted by nickel chloride hexahydrate for open-circuit voltage improvement in MAPbI₃ perovskite solar cells†

Pei Dong, Shuai Yuan, [ID] Dongping Zhu, [ID] Yaxin Du, Cheng Mu [ID] * and Xi-Cheng Ai [ID] *

SnO_2 is a promising electron transport layer (ETL) material with important applications in planar perovskite solar cells (PSCs). However, electron–hole recombination and charge extraction between SnO_2 and the perovskite layer necessitates further exploration. Nickel chloride hexahydrate ($NiCl_2 \cdot 6H_2O$) was introduced into the SnO_2 ETL, which significantly increased the power conversion efficiency (PCE) from 15.49 to 17.36% and the open-circuit voltage (V_{OC}) from 1.078 to 1.104 V. The improved PCE and V_{OC} were attributed to the reduced defect states and increased energy level of the conduction band minimum. This work provides new insights into optimizing the V_{OC} and PCE of PSCs.

Introduction

In recent years, the perovskite solar cell (PSC) has been developed as a promising type of solar cell with outstanding advantages such as high photoelectric conversion efficiency, low cost, and simple fabrication.[1–3] At present, PSCs have achieved a high power conversion efficiency (PCE) of 25.5%.[4–12] The main technical approach used to improve the PCE of PSCs is through component engineering of the perovskite layer, hole transport layer (HTL), and electron transport layer (ETL).[13–18] The other method is to optimize the interface performance by adjusting the structure or adding a buffer layer between the interlayers of PSCs.[19–28]

The quality of the ETL plays an important role in perovskite device performance. TiO_2, one of the most widely used ETL materials, has deep electron trap states, which easily leads to strong electron–hole recombination. ZnO has also been used as an ETL in PSCs due to its low-temperature film preparation and higher charge mobility. However, the PSC readily decomposes owing to the polyhydroxy groups on the surface of the ZnO. The SnO_2 ETL material is widely used in PSCs for high charge mobility and high perovskite compatibility.[29] However, the oxygen vacancy in SnO_2 greatly reduces the hole blocking effect, resulting in significant carrier recombination.[30] Therefore, the SnO_2 ETL requires modification to reduce ETL defects and improve the performance of PSCs. For example, Liu *et al.* incorporated EDTA into the SnO_2 ETL to enhance the device

Key Laboratory of Advanced Light Conversion Materials and Biophotonics, Department of Chemistry, Renmin University of China, Beijing 100872, China. E-mail: cmu@ruc.edu.cn; xcai@ruc.edu.cn

performance,[31] whereas Yang *et al.* doped Ga^{3+} ions into SnO_2 to passivate the defect state in the ETL.[32]

Herein, we report a simple and effective method to passivate SnO_2 defects by introducing nickel chloride hexahydrate ($NiCl_2 \cdot 6H_2O$) into a SnO_2 precursor solution. $NiCl_2 \cdot 6H_2O$ not only reduced the trap density, but also increased the energy level of the conduction band minimum of SnO_2 and caused the energy level to better match that of the perovskite. Consequently, a champion PCE of 17.36% with a V_{OC} of 1.104 V was achieved, remarkably higher than the relevant reference devices which provided a PCE of 15.49% and V_{OC} of 1.078 V.

Experimental section

Materials

All the materials and solvents were used as received without further purification. Fluorine-doped tin oxide (FTO) glasses (1.5 cm × 1.5 cm) were purchased from OPVtech (China). The SnO_2 solution (tin(IV) oxide, 15 wt% hydrocolloid dispersion) was purchased from Alfa Aesar. Lead iodide (PbI_2), methylammonium iodide (MAI), and 2,2',7,7'-tetrakis (*N*,*N*-di-*p*-methoxyphenylamine)-9,9'-spirobifluorene (spiro-OMeTAD) were obtained from Xi'an Polymer Light Technology. *N*,*N*-dimethylformamide (DMF), dimethyl sulfoxide (DMSO), chlorobenzene (CB), and 4-*tert*-butylpyridine were acquired from J&K. Lithium bis(trifluoromethylsulfonyl) imide (Li-TFSI) and cobalt(III) FK209 were obtained from Sigma-Aldrich. Nickel dichloride hexahydrate ($NiCl_2 \cdot 6H_2O$) and ammonium ($NH_3 \cdot H_2O$) were purchased from Aladdin.

Device fabrication

The FTO glass was sequentially cleaned with detergent water, deionized water, acetone, and isopropanol for 30 min in an

ultrasonic system. Plasma treatment was performed for 3 min to enhance the surface wettability before spin coating the ETL solution. The pristine SnO_2 precursor solution was prepared from the SnO_2 colloidal solution by diluting 5 times with deionized water. The sample ETL solution was prepared by adding 4, 12 and 20 mg $NiCl_2 \cdot 6H_2O$ into the 4 mL mixed solvent, which comprise of 1 mL SnO_2 colloidal solution, 2 mL H_2O and 1 mL $NH_3 \cdot H_2O$. Ultimately the concentration of the $NiCl_2 \cdot 6H_2O$ was 1, 3 and 5 mg mL^{-1}. The sample ETL (SnO_2–$NiCl_2$) solution was deposited on the FTO substrates at 4000 rpm for 30 s. The substrates were subsequently annealed in the air at 150 °C for 30 min to improve the electrical properties. After plasma treatment, the FTO substrates were transferred into a glove box. A perovskite precursor solution was prepared from the solution mixture of PbI_2 (1.67 M) and CH_3NH_3I (1.67 M) in DMF/DMSO (7 : 3 by volume). The perovskite solution was spin coated on the substrate at 1000 rpm for 13 s and at 5000 rpm for 25 s. Three hundred microliters of CB was dropped on the substrates during the second step after 12–15 s, and the films were then annealed on the hot plate at 100 °C for 30 min. After the substrates cooled to room temperature, a HTL was formed by spin coating the spiro-OMeTAD precursor solution onto the surface of the perovskite film at 5000 rpm for 30 s, which was prepared by dissolving 58.4 mg of spiro-OMeTAD, 23 μL of tBp, 14 μL of LiTFSI (520 mg mL^{-1} acetonitrile), and 23 μL of FK209 (300 mg mL^{-1} acetonitrile) in 800 μL of chlorobenzene. Finally, an 80 nm gold electrode was deposited on the surface of the HTL under high-vacuum conditions.

Measurements and characterization

Scanning electron microscopy (SEM) images were obtained by a field emission scanning electron microscope (FE-SEM, Hitachi SU8010). X-ray diffraction (XRD) was conducted on a Shimadzu XRD7000 diffractometer using Cu Kα radiation in the 2θ range from 10° to 60° at a scan rate of 2° min^{-1}. X-ray photoelectron spectroscopy (XPS) was performed using a Thermo KAlpha + instrument with an Al Kα (1486.8 eV) X-ray source. UV-vis absorption spectra were recorded on an Agilent Cary 60 spectrometer. Steady-state photoluminescence (PL) and time-resolved PL (TRPL) spectroscopies were performed by an Edinburgh FLS 980 spectrometer. The current density–voltage (J–V) curves were measured by a Keithley 2400 source meter under simulated standardized sunlight (AM 1.5 G, 100 mW cm^{-2}) in ambient air. The devices were covered by a metal aperture mask to determine the 0.1 cm^2 active area. The incident photon-to-current efficiency (IPCE) was characterized by the photoelectric conversion test system (Enlitech QE-R). Electrochemical impedance spectroscopy (EIS) was performed using ZAHNER PP211 with a frequency range from 0.1 to 10^6 Hz. The space charge limited current (SCLC) of the devices with FTO/SnO_2/perovskite/spiro/Au was measured on a Keithley 4200 from 0 to 2 V in the dark. In Transient photovoltage (TPV) measurements, the devices were illuminated by a light-emitting diode (LED, 520 ± 5 nm) to generate a different bias photovoltage (V_{ph}). A weak laser pulse (532 nm, 7 ns) was applied to generate a small perturbation. A series of desired V_{ph} values were collected by adjusting the intensity of the LED. The results were recorded using a digital oscilloscope (Lecroy HDO4054A, coupling impedance: 1 MΩ). Transient photocurrent (TPC) results were recorded using the digital oscilloscope (input impedance of 50 Ω) after the TPV measurements.

Results and discussion

As shown in Fig. S1,† the introduction of $NiCl_2 \cdot 6H_2O$ did not change the crystal structure of SnO_2. The higher transmittance of SnO_2–$NiCl_2$ film in the visible region indicates that $NiCl_2 \cdot 6H_2O$ could reduce the light loss when light passing through the substrate. FTO/SnO_2 films became smoother when the FTO substrate covered with a thin SnO_2 film. The smoother surface should be beneficial to the light transmission. SnO_2 films can improve the optical transmission properties of FTO substrates.[33,34] Compared with FTO/SnO_2, FTO/SnO_2–$NiCl_2$ films were denser, and Ni^{2+} had the effect of antireflection, which promoted the increase of transmittance of FTO/SnO_2–$NiCl_2$ films in the visible region.[35,36] Fig. 1a and b show the SEM images of the SnO_2 films without and with $NiCl_2$, respectively. The introduction of $NiCl_2 \cdot 6H_2O$ improved surface compactness of the ETL, which can promote the formation of perovskite grains and performance of the device.[37]

To confirm the successful introduction of nickel and chloride ions into the ETL, XPS was performed on different substrates. Fig. 1c shows the full XPS spectra of the corresponding ETLs. Fig. S4† shows energy dispersive spectroscopy (EDS) characterization of SnO_2–$NiCl_2$ films. The results show

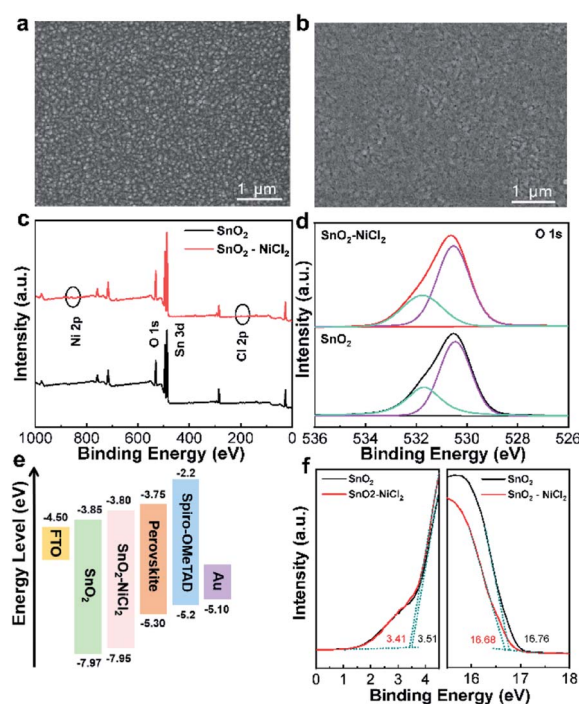**Fig. 1** ETLs using (a) pristine SnO_2 and (b) SnO_2–$NiCl_2$. (c) The XPS spectrum of SnO_2 and SnO_2–$NiCl_2$ on FTO substrates. (d) XPS of O 1s. (e) Energy level diagram of PSCs. (f) UPS spectra of SnO_2 and SnO_2–$NiCl_2$ films.

that the Ni, Cl, Sn, and O elements are uniformly distributed on the surface of the film. The enlarged XPS spectra are shown in Fig. S2 and S3†.[38] The XPS spectra of SnO_2–$NiCl_2$ show characteristic peaks of Ni (855 eV) and Cl (198 eV) compared with unmodified SnO_2. SnO_2 was deposited on FTO substrate, and it was annealed in the air at 150 °C for 30 min. In the annealing process, $[Ni(NH_3)_6]^{2+}$ by reaction with Ni^{2+} and $NH_3 \cdot H_2O$ would almost loses the NH_3 and H_2O when heated above 140 °C. The presence of Ni $2p_{3/2}$ at 855.6 eV, based on the binding energy position of XPS Ni 2p, indicates the transformation of Ni^{2+} into $Ni(OH)_2$. $Ni(OH)_2$ cannot further lose water to form NiO during annealing at 150 °C. The photoelectron binding energy of the Sn 3d level of SnO_2–$NiCl_2$ is slightly higher than that of the unmodified SnO_2, indicating an interaction between SnO_2 and $NiCl_2$. According to previous reports, the Ni^{2+} may play a more important role than Cl^- in improving the device performance of PSCs.[39] We presumed that the Ni^{2+} from $NiCl_2$ can interact with the hydroxyl groups (-OH) on the surface of the SnO_2 film, which can lead to a trap state, causing nonradiative recombination.[40] As shown in Fig. 1d and Table S1,† the peak at 530.46 eV was O–Sn bonds (or O^{2-} state), and the higher binding energy at 531.70 eV corresponded to hydroxyl groups (or oxygen vacancies). After the introduction of $NiCl_2 \cdot 6H_2O$, the intensity of hydroxyl (or oxygen vacancies) decreased significantly, indicating that the oxygen vacancies were effectively passivated.[41] The reduction of oxygen vacancy defects will improve V_{OC}. Therefore, the successful introduction of $NiCl_2 \cdot 6H_2O$ will considerably improve the ETL.

Further characterizations were conducted to better understand the ETL/perovskite interface. Ultraviolet photoelectron spectroscopy (UPS) was performed to investigate the band structure of SnO_2 and SnO_2–$NiCl_2$. We tested the optimal concentration 3 mg mL^{-1}. The possible energy band alignment of planar PSCs was depicted in Fig. 1e. Combining with the high binding energy cutoff (E_{cutoff}) on the right side of Fig. 1f and the Fermi edge ($E_{F,edge}$) region on the left side of Fig. 1f, the value of E_{VB} could be calculated for SnO_2 and SnO_2–$NiCl_2$ at about -7.97 and -7.95 eV, respectively. We further confirmed the band gaps (E_g) of ETLs by the Tauc plots of UV-vis absorption spectra (Fig. S5†). The energy levels of the conduction band (E_{CB}) of SnO_2 and SnO_2–$NiCl_2$ were calculated to be -3.85 and -3.80 eV, respectively. According to the relative energy levels of the different PSC parts, the E_{CB} of the SnO_2–$NiCl_2$ ETL was higher than that of the SnO_2 ETL.[42] The V_{OC} depends on the difference in energy between electron quasi Fermi level and hole quasi Fermi level.[43] More appropriate energy level would make the solar cell based on SnO_2–$NiCl_2$ show higher V_{OC}.

SEM characterization of the perovskite films prepared on SnO_2 and SnO_2–$NiCl_2$ substrates was performed, and the results are shown in Fig. 2a and b. The perovskite films prepared on the SnO_2–$NiCl_2$ substrates have larger grains and are generally compact, compared with the perovskite films prepared on SnO_2. In addition, cracks obviously exist on the perovskite films prepared on SnO_2, which lead to the recombination of electrons and holes.[44] The UV-vis absorption spectrum shown in Fig. 2c indicates that the bandgap of perovskite growing on the $NiCl_2$-modified ETL has not changed. Fig. S6† presents the bandgap of
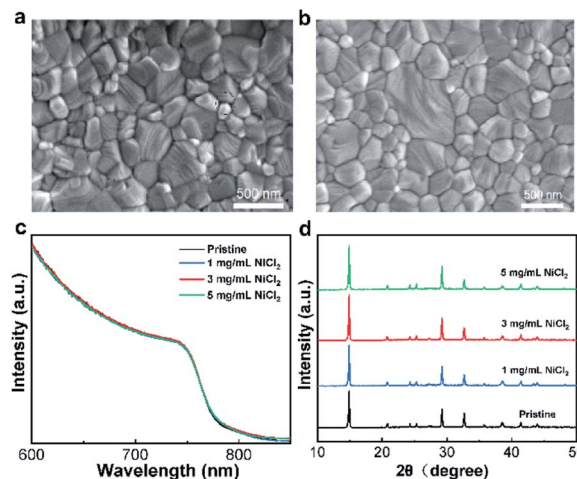

Fig. 2 Top view SEM images of perovskite films (a) with pristine SnO_2 and (b) SnO_2–$NiCl_2$. (c) The absorbance of perovskite films based on SnO_2 and SnO_2–$NiCl_2$. (d) The XRD pattern of perovskite films with different concentrations of SnO_2–$NiCl_2$.

perovskite grown on ETL with and without $NiCl_2 \cdot 6H_2O$, and the calculated bandgap value is 1.61 eV. XRD analyses were performed to characterize the crystal structure of perovskite, as shown in Fig. 2d. The results show that the characteristic diffraction peaks of $CH_3NH_3PbI_3$ appear near 14.1°, 24.5°, 28.5°, 31.6°, and 40.4°, which correspond to the crystal planes of (110), (202), (220), (310), and (224) of $CH_3NH_3PbI_3$, respectively.[45,46] These results confirm that perovskite films with good crystallinity were prepared by introducing $NiCl_2 \cdot 6H_2O$.

To study the carrier transport in PSCs, steady-state fluorescence spectroscopy (PL) experiments were performed on the perovskite films on SnO_2 and SnO_2–$NiCl_2$ substrates.[47,48] As shown in Fig. 3a, carrier quenching was slower for the samples on the SnO_2–$NiCl_2$ substrates, which is detrimental to increasing J_{SC} of the solar cell. However, the transmittance of the tin dioxide layer was increased after modification by $NiCl_2 \cdot 6H_2O$, the utilization rate of photons will be improved and J_{SC} will increase. Overall, the J_{SC} of the device based on SnO_2–$NiCl_2$ was a little better than that of the SnO_2 solar cell. The reason of the carrier quenching was slow for the samples on he SnO_2–$NiCl_2$ substrates was the passivation of chloride ions, which suppressed the nonradiative recombination of perovskite films for the enhancing intensity and the larger perovskite grain
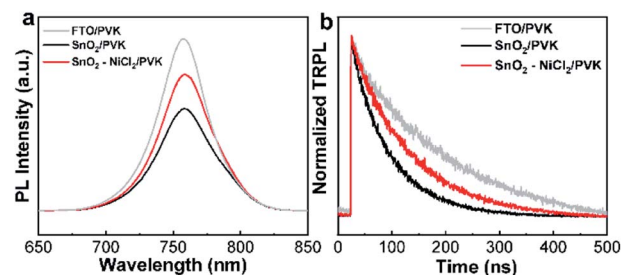

Fig. 3 (a) The PL and (b) TRPL spectra of $MAPbI_3$ without and with $NiCl_2$.

size.[40] In Fig. 3b, the biexponential decay behavior is evident on the TRPL spectrum. We calculated the decay times (*e.g.*, τ_1 and τ_2) of the perovskite film deposited on the SnO_2 and SnO_2–$NiCl_2$ substrates; the fitting parameters are summarized in Table S2.† PL decay process consists of a carrier recombination process in the bulk region, as characterized by the slow decay lifetime τ_2, as well as a charge-transfer process at the interface, as characterized by the fast lifetime τ_1. According to the results of the double exponential fitting in TRPL τ_1 increases, show that charge extraction at a slower pace and it will cause a decline in J_{SC}. τ_2 increases, and combining with SCLC and EIS data, shows that tin oxide layer of oxygen vacancy defects passivation, V_{OC} increases. The average decay time of the SnO_2/perovskite film is 70.62 ns, and the perovskite film deposited on SnO_2–$NiCl_2$ exhibited slower fluorescence quenching with an average decay time of 107.1 ns. The results were consistent with PL conclusions.

To justify the photoelectric performance of the PSCs caused by the introduction of $NiCl_2 \cdot 6H_2O$, SCLC analyses were performed on the SnO_2 and SnO_2–$NiCl_2$ ETLs. The results are shown in Fig. 4a and b, including the calculated density of defect states. The defect density between the interface of ETL and the perovskite layer can partially reflect the contact and matching degree between interfaces. In the SCLC analyses, there is a clear linear relationship between the current and low bias voltage, which becomes non-linear as the voltage increases. The bias voltage of different substrates can be obtained from the SCLC curve, and the defect density can be subsequently calculated according to the formula of $N_t = 2\varepsilon\varepsilon_0 V_{TFL}/eL^2$, where V_{TFL} is the trap-filled-limit voltage marked in Fig. 4a and b, e is the elementary charge, L is the thickness of the perovskite film, ε is the dielectric constant, and ε_0 is the vacuum permittivity. According to the single calculation of the SCLC results, the bias voltage of the SnO_2–$NiCl_2$ substrate decreased from 0.930 V to 0.810 V, indicating a tendency of the defect state between the ETL and the perovskite layer to decrease after $NiCl_2$ modification. After further calculation obtained defect concrete values, the trap

densities of perovskite film deposited on pristine SnO_2 and SnO_2–$NiCl_2$ ETL are $1.45 \times 10^{16} \text{ cm}^{-3}$ and $1.26 \times 10^{16} \text{ cm}^{-3}$.

We further elucidated the effect of $NiCl_2$ on the defects of the SnO_2 film by measuring the recombination dynamics, transient photovoltage (TPV), and transient photocurrent (TPC) decay. As shown in Fig. 4c, the carrier recombination lifetime of the device with SnO_2–$NiCl_2$ increased from 22.65 to 35.33 μs, confirming the suppressed charge recombination at the ETL and perovskite interface. For the transport time constants (τ_t) measured from TPC (Fig. 4d), PSCs based on SnO_2–$NiCl_2$ exhibited 0.67 μs compared to that of the pristine SnO_2-based PSCs (0.93 μs).[49,50]

To investigate the effect of SnO_2–$NiCl_2$ ETL on device performance, we fabricated PSCs with the FTO/ETL/MAPbI$_3$/Spiro-OMeTAD/Au (Fig. 5a) structure and investigated the doping concentration of $NiCl_2 \cdot 6H_2O$ in SnO_2. The devices were prepared with the concentration of SnO_2 precursor solution (1, 3 and 5 mg mL^{-1}) and annealing at 150 °C for 30 min. Electrochemical impedance spectroscopy (EIS) analyses were performed on devices composed of SnO_2 and SnO_2–$NiCl_2$ substrates,[51–53] and the results are shown in Fig. 5b. In the dark state condition, within the frequency range of 0.1 to 10^6 Hz, the transmission electricity of the SnO_2-based cell was measured. By fitting the measured results, the contact resistance (R_s) and recombination resistance (R_{rec}) values of the PSCs employing pristine SnO_2 and SnO_2–$NiCl_2$ are summarized in Table S3.† The small semicircle at high frequency corresponds to the charge transfer process between perovskite and selective
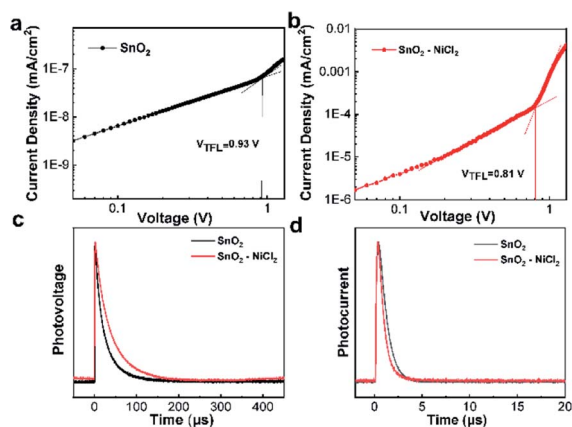

Fig. 4 SCLC measurements of devices (a) with pristine SnO_2 and (b) SnO_2–$NiCl_2$. (c) Transient photovoltage decay curves of PSCs based on pristine SnO_2 and SnO_2–$NiCl_2$. (d) Transient photocurrent decay curves of PSCs based on pristine SnO_2 and SnO_2–$NiCl_2$.

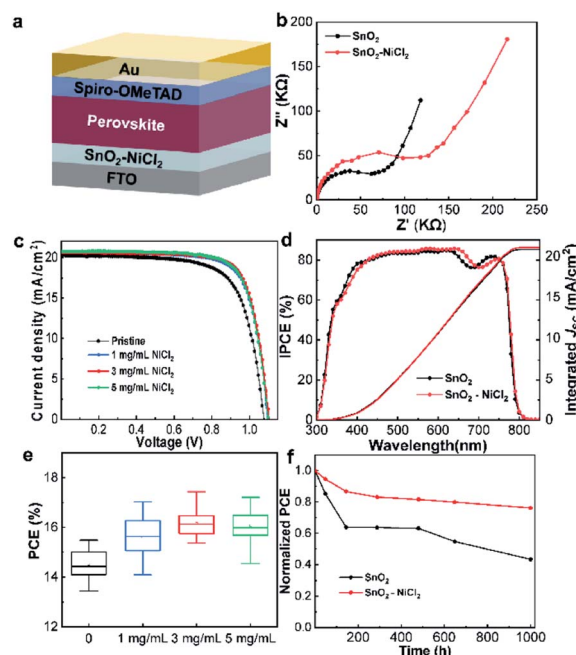**Fig. 5** (a) Device architecture. (b) Nyquist plots. (c) $J-V$ characteristics of the best devices with different nickel chloride concentrations. (d) External quantum efficiency of PSCs based on pristine SnO_2 and SnO_2–$NiCl_2$. (e) Device performance of PSCs based on SnO_2 with different concentrations of $NiCl_2$. (f) Stability measurements of PSCs based on pristine SnO_2 and SnO_2–$NiCl_2$ under a N_2 atmosphere.

Table 1 Photovoltaic parameters of cells based on SnO_2 and SnO_2–$NiCl_2$ films with different additive concentrations

Samples	V_{OC} (V)	J_{SC} (mA cm^{-2})	FF (%)	PCE (%)
Pristine	1.078	20.21	0.711	15.49
1 mg mL^{-1} $NiCl_2$	1.098	20.70	0.749	17.02
3 mg mL^{-1} $NiCl_2$	1.104	20.59	0.764	17.36
5 mg mL^{-1} $NiCl_2$	1.100	20.70	0.756	17.21

contacts while the large semicircle at low frequency demonstrates the recombination of charge carriers in the perovskite layer.[54] Through EIS test, the results show that the transmission resistance R_s and the composite resistance R_{rec} increased, indicating that the charge transmission speed slowed down and the defect was effectively passivated. However, because the transmittance of the tin dioxide layer increased after modification, the utilization rate of photons will be improved and J_{SC} will increase. The results were consistent with the fluorescence and efficiency data.[52] Simultaneously, it was beneficial to improve V_{OC} of the device.[53]

The corresponding J–V curves are shown in Fig. 5c and S7.† The results show that the device performance slightly improved with SnO_2–$NiCl_2$ concentration of 1 mg mL^{-1}. The highest open-circuit voltage (V_{OC}), FF, and PCE values of the PSCs were obtained with SnO_2–$NiCl_2$ concentration of 3 mg mL^{-1}. When the doping $NiCl_2 \cdot 6H_2O$ amount further increased, the photoelectric performance of the device decreased, and thus the optimum concentration of SnO_2–$NiCl_2$ was 3 mg mL^{-1}.

Subsequently, the IPCE of the optimum $NiCl_2 \cdot 6H_2O$ and control devices were tested. As shown in Fig. 5d, the light absorption capacity of the $NiCl_2$-modified devices in the range of 400–700 nm was stronger than that of the SnO_2-based devices, corresponding to a higher current. The results show that the introduction of $NiCl_2 \cdot 6H_2O$ could effectively improve the ability of the ETL to light transmission. The integrated J_{SC} value measured by IPCE was consistent with the J_{SC} obtained by the J–V curves.

The statistical distribution of PCE for PSCs based on doped ETLs of different $NiCl_2 \cdot 6H_2O$ concentrations are shown in Fig. 5e and S8.† The PCE of the SnO_2-based devices ranged between 14%-16% and the PCE of the SnO_2–$NiCl_2$-based devices was in the range of 16–18%. As shown in Table 1, the modified device exhibits a PCE of 17.36% with a J_{SC} of 20.59 mA cm^{-2}, V_{OC} of 1.104 V, and FF of 76.4%. Devices based on the SnO_2–$NiCl_2$ ETL also exhibit greater stability than the reference devices (Fig. 5f). The SnO_2–$NiCl_2$-based PSCs can retain 76% of their initial efficiency after being stored for 1000 h at the room temperature (RT) of 25 °C for 1000 h. In contrast, the reference devices only retained 43% of their initial efficiency. This may be due to the larger grain size with fewer grain boundaries which offers additional protection against oxygen and moisture.

Conclusions

In this study, we provide a simple and effective method to modify SnO_2 ETL with $NiCl_2 \cdot 6H_2O$, which reduced the oxygen vacancies of SnO_2 and improved the energy level alignment.

This modification ultimately dramatically passivated defects, which effectively improved the V_{OC} and PCE. Notably, the stability of the SnO_2–$NiCl_2$-based PSCs increased, and was able to maintain 76% of the original PCE after 1000 h of storage, compared to 43% for the device without $NiCl_2 \cdot 6H_2O$.

Conflicts of interest

There are no conflicts to declare.

Acknowledgements

Notes and references

1 Q. Chen, N. De Marco, Y. Yang, T.-B. Song, C.-C. Chen, H. Zhao, Z. Hong, H. Zhou and Y. Yang, *Nano Today*, 2015, **10**, 355–396.

2 M. A. Green, A. Ho-Baillie and H. J. Snaith, *Nat. Photonics*, 2014, **8**, 506–514.

3 G. Xing, N. Mathews, S. Sun, S. S. Lim, Y. M. Lam, M. Gratzel, S. Mhaisalkar and T. C. Sum, *Science*, 2013, **342**, 344–347.

4 H. Min, M. Kim, S. U. Lee, H. Kim, G. Kim, K. Choi, J. H. Lee and S. I. Seok, *Science*, 2019, **366**, 749–753.

5 M. Abdi-Jalebi, Z. Andaji-Garmaroudi, S. Cacovich, C. Stavrakas, B. Philippe, J. M. Richter, M. Alsari, E. P. Booker, E. M. Hutter, A. J. Pearson, S. Lilliu, T. J. Savenije, H. Rensmo, G. Divitini, C. Ducati, R. H. Friend and S. D. Stranks, *Nature*, 2018, **555**, 497–501.

6 W. S. Yang, B. W. Park, E. H. Jung, N. J. Jeon, Y. C. Kim, D. U. Lee, S. S. Shin, J. Seo, E. K. Kim, J. H. Noh and S. I. Seok, *Science*, 2017, **356**, 1376–1379.

7 W. S. Yang, J. H. Noh, N. J. Jeon, Y. C. Kim, S. Ryu, J. Seo and S. I. Seok, *Science*, 2015, **348**, 1234–1237.

8 K. Xiao, R. Lin, Q. Han, Y. Hou, Z. Qin, H. T. Nguyen, J. Wen, M. Wei, V. Yeddu, M. I. Saidaminov, Y. Gao, X. Luo, Y. Wang, H. Gao, C. Zhang, J. Xu, J. Zhu, E. H. Sargent and H. Tan, *Nat. Energy*, 2020, **5**, 870–880.

9 M. Jeong, I. W. Choi, E. M. Go, Y. Cho, M. Kim, B. Lee, S. Jeong, Y. Jo, H. W. Choi, J. Lee, J. H. Bae, S. K. Kwak, D. S. Kim and C. Yang, *Science*, 2020, **369**, 1615–1620.

10 R. Lin, K. Xiao, Z. Qin, Q. Han, C. Zhang, M. Wei, M. I. Saidaminov, Y. Gao, J. Xu, M. Xiao, A. Li, J. Zhu, E. H. Sargent and H. Tan, *Nat. Energy*, 2019, **4**, 864–873.

11 M. Saliba, T. Matsui, J. Y. Seo, K. Domanski, J. P. Correa-Baena, M. K. Nazeeruddin, S. M. Zakeeruddin, W. Tress, A. Abate, A. Hagfeldt and M. Gratzel, *Energy Environ. Sci.*, 2016, **9**, 1989–1997.

12 H. Min, D. Y. Lee, J. Kim, G. Kim, K. S. Lee, J. Kim, M. J. Paik, Y. K. Kim, K. S. Kim, M. G. Kim, T. J. Shin and S. Il Seok, *Nature*, 2021, **598**, 444–450.

13 W. Xu, X. Yao, H. Wu, T. Zhu and X. Gong, *Emergent Mater.*, 2020, **3**, 727–750.

14 X. Zhao, L. Tao, H. Li, W. Huang, P. Sun, J. Liu, S. Liu, Q. Sun, Z. Cui, L. Sun, Y. Shen, Y. Yang and M. Wang, *Nano Lett.*, 2018, **18**, 2442–2449.

15 Y. Wu, X. Yang, W. Chen, Y. Yue, M. Cai, F. Xie, E. Bi, A. Islam and L. Han, *Nat. Energy*, 2016, **1**, 16148.

16 Z. Zhu, C. C. Chueh, F. Lin and A. K. Jen, *Adv. Sci. (Weinh.)*, 2016, **3**, 1600027.

17 G. Grancini, C. Roldan-Carmona, I. Zimmermann, E. Mosconi, X. Lee, D. Martineau, S. Narbey, F. Oswald, F. De Angelis, M. Graetzel and M. K. Nazeeruddin, *Nat. Commun.*, 2017, **8**, 15684.

18 P. W. Liang, C. Y. Liao, C. C. Chueh, F. Zuo, S. T. Williams, X. K. Xin, J. Lin and A. K. Jen, *Adv. Mater.*, 2014, **26**, 3748–3754.

19 C. Zuo and L. Ding, *Nanoscale*, 2014, **6**, 9935–9938.

20 W. Ke, C. Xiao, C. Wang, B. Saparov, H. S. Duan, D. Zhao, Z. Xiao, P. Schulz, S. P. Harvey, W. Liao, W. Meng, Y. Yu, A. J. Cimaroli, C. S. Jiang, K. Zhu, M. Al-Jassim, G. Fang, D. B. Mitzi and Y. Yan, *Adv. Mater.*, 2016, **28**, 5214–5221.

21 Y. Wu, F. Xie, H. Chen, X. Yang, H. Su, M. Cai, Z. Zhou, T. Noda and L. Han, *Adv. Mater.*, 2017, **29**, 1701073.

22 F. Wang, W. Geng, Y. Zhou, H. H. Fang, C. J. Tong, M. A. Loi, L. M. Liu and N. Zhao, *Adv. Mater.*, 2016, **28**, 9986–9992.

23 H. S. Kim, C. R. Lee, J. H. Im, K. B. Lee, T. Moehl, A. Marchioro, S. J. Moon, R. Humphry-Baker, J. H. Yum, J. E. Moser, M. Gratzel and N. G. Park, *Sci. Rep.*, 2012, **2**, 591.

24 M. M. Lee, J. Teuscher, T. Miyasaka, T. N. Murakami and H. J. Snaith, *Science*, 2012, **338**, 643–647.

25 R. Meng, X. Feng, Y. Yang, X. Lv, J. Cao and Y. Tang, *ACS Appl. Mater. Interfaces*, 2019, **11**, 13273–13278.

26 A. K. Kadhim, M. R. Mohammad and A. I. Abd Ali, *Chem. Phys. Lett.*, 2022, **786**, 139189.

27 G. Liu, Z. Liu, L. Wang, K. Zhang and X. Xie, *Chem. Phys. Lett.*, 2021, **771**, 138496.

28 F. Wang, M. Yang, Y. Zhang, J. Du, S. Yang, L. Yang, L. Fan, Y. Sui, Y. Sun and J. Yang, *Nano Res.*, 2021, **14**, 2783–2789.

29 Q. Zhuang, H. Wang, C. Zhang, C. Gong, H. Li, J. Chen and Z. Zang, *Nano Res.*, 2022, DOI: **10.1007/s12274-022-4135-7**.

30 S. Wendt, P. T. Sprunger, E. Lira, G. K. Madsen, Z. Li, J. O. Hansen, J. Matthiesen, A. Blekinge-Rasmussen, E. Laegsgaard, B. Hammer and F. Besenbacher, *Science*, 2008, **320**, 1755–1759.

31 D. Yang, R. Yang, K. Wang, C. Wu, X. Zhu, J. Feng, X. Ren, G. Fang, S. Priya and S. F. Liu, *Nat. Commun.*, 2018, **9**, 3239.

32 T. Yang, X. Qin, H.-h. Wang, Q. Jia, R. Yu, B. Wang, J. Wang, K. Ibrahim, X. Jiang and Q. He, *Thin Solid Films*, 2010, **518**, 5542–5545.

33 W. Ke, G. Fang, Q. Liu, L. Xiong, P. Qin, H. Tao, J. Wang, H. Lei, B. Li, J. Wan, G. Yang and Y. Yan, *J. Am. Chem. Soc.*, 2015, **137**, 6730–6733.

34 Y. Luan, X. Yi, P. Mao, Y. Wei, J. Zhuang, N. Chen, T. Lin, C. Li and J. Wang, *iScience*, 2019, **16**, 433–441.

35 Y. Chen, X. Zuo, Y. He, F. Qian, S. Zuo, Y. Zhang, L. Liang, Z. Chen, K. Zhao, Z. Liu, J. Gou and S. F. Liu, *Adv. Sci. (Weinh.)*, 2021, **8**, 2001466.

36 Z. Qian, L. Chen, J. Wang, L. Wang, Y. Xia, X. Ran, P. Li, Q. Zhong, L. Song, P. Müller-Buschbaum, Y. Chen and H. Zhang, *Adv. Mater. Interfaces*, 2021, **8**, 2100128.

37 B. Y. Gao, Q. Cao, X. Y. Pu, J. B. Yang, J. Han, S. J. Wang, T. T. Li, Z. W. He and X. H. Li, *Appl. Surf. Sci.*, 2021, **546**, 148711.

38 L. Zhu, Q. Lu, C. Li, Y. Wang and Z. Deng, *Chin. Chem. Lett.*, 2021, **32**, 2259–2262.

39 D. Wang, C. Wu, X. Qi, W. Luo, Y. Zhang, Z. Zhang, X. Guo, B. Qu, L. Xiao and Z. Chen, *ACS Appl. Energy Mater.*, 2019, **2**, 5883–5888.

40 P. Wang, B. Chen, R. Li, S. Wang, N. Ren, Y. Li, S. Mazumdar, B. Shi, Y. Zhao and X. Zhang, *ACS Energy Lett.*, 2021, **6**, 2121–2128.

41 D. Wang, T. He, S. Li, Y. Jiang and M. Yuan, *ACS Appl. Energy Mater.*, 2021, DOI: **10.1021/acsaem.1c02666**.

42 J. Yan, Z. Lin, Q. Cai, X. Wen and C. Mu, *ACS Appl. Energy Mater.*, 2020, **3**, 3504–3511.

43 P. Caprioglio, M. Stolterfoht, C. M. Wolff, T. Unold, B. Rech, S. Albrecht and D. Neher, *Adv. Energy Mater.*, 2019, **9**, 1901631.

44 X. Liu, Y. Zhang, L. Shi, Z. Liu, J. Huang, J. S. Yun, Y. Zeng, A. Pu, K. Sun, Z. Hameiri, J. A. Stride, J. Seidel, M. A. Green and X. Hao, *Adv. Energy Mater.*, 2018, **8**, 1800138.

45 S. Sidhik, A. Cerdan Pasaran, D. Esparza, T. Lopez Luke, R. Carriles and E. De la Rosa, *ACS Appl. Mater. Interfaces*, 2018, **10**, 3571–3580.

46 J. Cao, X. Lv, P. Zhang, T. T. Chuong, B. Wu, X. Feng, C. Shan, J. Liu and Y. Tang, *Adv. Mater.*, 2018, **30**, e1800568.

47 M. Kim, G.-H. Kim, T. K. Lee, I. W. Choi, H. W. Choi, Y. Jo, Y. J. Yoon, J. W. Kim, J. Lee, D. Huh, H. Lee, S. K. Kwak, J. Y. Kim and D. S. Kim, *Joule*, 2019, **3**, 2179–2192.

48 M. Sun, J. Shu, C. Zhao, J. Wu, H. Guo, Y. Guo, X. Yin, Y. Lin, Z. Tan, M. He and L. Wang, *ACS Appl. Mater. Interfaces*, 2022, **14**, 13352–13360.

49 J. W. Jung, S. T. Williams and A. K. Y. Jen, *RSC Adv.*, 2014, **4**, 62971–62977.

50 Y. Liu, Q. Chen, H.-S. Duan, H. Zhou, Y. Yang, H. Chen, S. Luo, T.-B. Song, L. Dou, Z. Hong and Y. Yang, *J. Mater. Chem. A*, 2015, **3**, 11940–11947.

51 K. Liu, S. Chen, J. Wu, H. Zhang, M. Qin, X. Lu, Y. Tu, Q. Meng and X. Zhan, *Energy Environ. Sci.*, 2018, **11**, 3463–3471.

52 H. S. Kim, J. W. Lee, N. Yantara, P. P. Boix, S. A. Kulkarni, S. Mhaisalkar, M. Gratzel and N. G. Park, *Nano Lett.*, 2013, **13**, 2412–2417.

53 T. Zhu, Y. Yang, S. Zhou, X. Yao, L. Liu, W. Hu and X. Gong, *Chin. Chem. Lett.*, 2020, **31**, 2249–2253.

54 N. D. Pham, V. T. Tiong, P. Chen, L. Wang, G. J. Wilson, J. Bell and H. Wang, *J. Mater. Chem. A*, 2017, **5**, 5195–5203.